Published in final edited form as:
J Biomed Opt. 2008 ; 13(2): 021108. doi:10.1117/1.2892687.

Optical clearing in transcutaneous Raman spectroscopy of murine cortical bone tissue

Matthew V. Schulmerich[a], **Jacqueline H. Cole**[a], **Kathryn A. Dooley**[a], **Jaclynn M. Kreider**[b], **Steven A. Goldstein**[b], and **Michael D. Morris**[a]

[a]Department of Chemistry, University of Michigan, Ann Arbor, MI 48109, USA

[b]Orthopaedic Research Laboratory, Department of Orthopaedic Surgery, University of Michigan Medical School, Ann Arbor, MI 48109

Abstract

The effect of optical clearing with glycerol on the Raman spectra of bone tissue acquired transcutaneously on right and left tibiae from four mice was studied. Multiple transcutaneous measurements were obtained from each limb; glycerol was then applied as an optical clearing agent, and additional transcutaneous measurements were taken. Glycerol reduces the noise in the raw spectra ($p=0.0037$) and significantly improves the cross-correlation between the recovered bone factor and the exposed bone measurement in a low signal-to-noise region of the bone spectra ($p=0.0245$).

Keywords

Transcutaneous; optical clearing; Raman Spectroscopy; Bone; Fiber Optic Probe

1 Introduction

Raman spectroscopy is a potential non-invasive measurement technique for longitudinal studies of bone development[1, 2], bone biomechanics[3–5] in humans and in animals, and diagnosis of bone diseases.[6–9] To realize this potential it is necessary to develop both spectroscopic instrumentation for transcutaneous measurements of bone tissue composition and ancillary techniques, such as optical clearing,[10] that enhance the recovery of subsurface spectra. Skin presents a formidable barrier to bone Raman spectroscopy, both because the tissue, especially the stratum corneum, is highly scattering, and because melanocytes, which contain the skin pigment melanin, absorb even in the near-infrared (NIR) spectrum and fluoresce intensely. Raman spectroscopy has been used to study skin and skin diseases.[11–13] To date, dermatological Raman spectroscopy has aimed primarily to measure the moisture content and drug penetration in skin at depths that do not exceed 1 mm.[14, 15] Similarly, arterial plaque[16–18] and blood components[12, 19–21] have been measured using arteries that lie close to the surface of the skin.

Although it has not previously been applied to Raman spectroscopy, optical clearing is well-known in other areas of biomedical optics, including NIR spectroscopy and optical coherence tomography.[10, 22–25] With this methodology, a liquid is used to penetrate the stratum corneum and displace the native water, because it has an index of refraction that is closer to that of proteins. Clearing agents may also disrupt the internal hydrogen bonding of collagen, which

Correspondence to: Michael D. Morris.

partially disorders the fibrils and increases their transparency.[22, 26] The use of an optical clearing agent decreases scattering, thereby increasing light penetration into the tissue.[10] Glycerol is one of the most commonly employed clearing agents. It is non-toxic, has a high index of refraction (n_D = 1.47) and disrupts the internal hydrogen bonding of collagen. For these reasons we have used glycerol in this study.

With the development of spatially-resolved Raman spectroscopy,[27, 28] transcutaneous measurements at depths of several millimeters or greater have become feasible. In human cadaveric tissue, we have shown that transcutaneous bone Raman spectra can be obtained with a commercially available fiber optic probe that uses distributed laser power and an array of collection fibers.[29, 30] Using a recently developed ring/disk probe,[31–33] we have demonstrated the recovery of Raman spectra from canine bone tissue at a depth of 5 mm below the skin surface.[34] This work demonstrated several difficulties that must be addressed in the development of non-invasive bone Raman spectroscopy. These include a high background fluorescence, multiple scattering that is characteristic of almost all tissue,[35–37] and the limitations of existing fiber optic Raman probes.

In this communication we discuss the use of optical clearing to improve the Raman signal and reduce the effects of scattering. We show that a very simple protocol with glycerol as a clearing agent increases the signal-to-noise ratio and reduces the systematic error incurred as a result of incompletely resolved surface and subsurface spectra using multivariate techniques. We also demonstrate a fiber probe with line-focused laser delivery that is better suited to small animal limb studies than ring-focused probes.

2 Materials and Methods

2.1 Specimens and Reagents

The specimens used for *in vitro* transcutaneous Raman measurements through skin and overlying tissue were tibiae from mice sacrificed between the ages of 12 and 20 weeks in the course of other unrelated studies. These mice were sacrificed according to study designs and protocols approved by the University of Michigan Committee on Use and Care of Animals. Both tibiae from healthy female animals from four randomly selected mice strains were used.

The depilatory agent was Sally Hansen Hair Removal Lotion (Sally Hansen Corp, Uniondale, NY.). The optical clearing agent was American Chemical Society reagent grade glycerol (Sigma-Aldrich Corp., Milwaukee, WI).

2.2 Instrumentation

A schematic of the Raman instrument is shown in Figure 1. A 400 mW, 785 nm external cavity diode laser (Invictus, Kaiser Optical Systems, Inc., Ann Arbor, MI) was used for excitation. The laser beam was passed through a 200 μm core NIR optical fiber (PCN200 4-FF-HT-GN, Multimode Fiber Optics, Hackettstown, NJ). The light was collimated with a fiber optic collimator (F230FC-B, Thorlabs Inc., Newton, NJ) and directed through a 5° fan angle Powell lens/collimating optics assembly (C10, StockerYale Montreal, Quebec, Canada) and a 75 mm focal length NIR coated achromat (AC254-075-B, Thorlabs Inc., Newton, NJ) to obtain a 3 mm by 0.75 mm line illumination. A non-confocal fiber optic probe (PhAT probe, Kaiser Optical Systems, Inc.) was employed to collect backscattered Raman shifted light and present it to the spectrograph. The probe contained a circular bundle of fifty 100 μm core collection fibers. At the probe head a 75 mm focal length lens was employed to obtain a 3 mm diameter circular field of view. A dichroic mirror (Chroma Technology Corp., Rockingham, VT) reflected the 785 nm light to the sample and transmitted the Raman signal to the collection fibers. A NIR-optimized imaging spectrograph (HoloSpec f/1.8i, Kaiser Optical Systems)

fitted with a 50 μm slit was used to provide a 6–8 cm^{-1} spectral resolution. The detector was a thermoelectrically cooled, deep-depletion 1024x256 pixel charged-coupled device camera (CCD) (DU420-BR-DD, Andor Technology, Belfast, Northern Ireland) operated at −75°C with no binning.

2.3 Spectroscopic Measurements

Transcutaneous Raman spectroscopic measurements were made on intact, sacrificed animals. Prior to measurement, the depilatory lotion was used on the tibiae to facilitate hair removal with a tissue paper wipe from the region of interest. Excess depilatory was rinsed off with distilled water after hair removal was complete. After transcutaneous measurements, the entire tibia was excised, and overlying tissue was removed with a scalpel. The Raman spectrum of the exposed bone was then measured in the same region.

Transcutaneous Raman spectra were acquired with the illumination line and the collection disk focused onto the skin at the medial side of the tibia mid-diaphysis just below the tibial proximal tuberosity. The laser line was positioned so that the long axis of the line was parallel to the bone and centered over the bone. The power of the laser light at the specimen was 35 mW. The acquisition time was 300 s for transcutaneous measurements and 120s for exposed bone measurements. For optical clearing experiments, glycerol was applied topically with a cotton swab. The glycerol was left to diffuse into the skin for approximately three minutes before spectra were acquired.

For six of the tibiae, seven sequential replicate spectra were acquired prior to optical clearing. After application of glycerol and a three minute wait, seven replicate spectra were acquired in the same location. For one of the tibiae, only five measurements were taken before optical clearing and five afterwards. After the sequence of transcutaneous measurements was completed, soft tissue was removed, and twenty consecutive Raman spectra of the exposed bone were acquired.

2.4 Data Analysis

Data reduction was performed in MATLAB 6.1 (The Mathworks Inc., Natick, MA) using vendor-supplied scripts and locally-written scripts that have been described previously. Statistical analyses were performed in SAS, version 9.1 (SAS Institute Inc., Cary, NC).

A single CCD frame contained 256 Raman spectra. Initial preprocessing included CCD calibration against a neon discharge lamp, with a check against a Teflon® Raman spectrum. White light correction and dark current subtraction were used to account for the spectral response of the detector. The image was then corrected for curvature caused by the large gathering angle of the spectrograph.

The spectrum from each of the fifty collection fibers of the probe was imaged onto slightly more than 5 rows of the CCD. To avoid cross-talk, spectra from only the central three rows of each fiber image were used. These three spectra were averaged to generate one spectrum for each collection fiber. Finally, the 905–1500 cm^{-1} region of interest (ROI) was selected. This region contains the mineral phosphate P-O and carbonate C-O stretches and matrix bands including collagen amide III and CH_2 wag.[2, 8, 38]

The amount of noise in the transcutaneous measurements was quantified using spectral averages, that is, without background correction and without separation into bone and overlying tissue components. The three spectra from each of the fifty collection fibers were averaged, and the power spectrum of each averaged spectrum was computed. For this purpose, the dispersion axis was not converted to wavenumber, but was left in wavelength (nm) so that the noise contribution from each pixel would be equally weighted. The root-mean-square (rms)

value was calculated for the high transform frequency region between 0.02 cycles/nm and 0.07 cycles/nm. Data from one tibia was excluded, because the probe was improperly aligned during the measurements. For each of the remaining six tibiae, the mean rms values were computed for each of the seven sequential acquisitions.

For each tibia, a paired t-test was used to assess the difference in rms noise magnitudes between spectra of each tibia acquired with and without optical clearing. The effect of optical clearing on the noise rms values was examined for all six tibiae using a repeated measures analysis of variance (ANOVA). Using a mixed-effects model[39], optical clearing was treated as a fixed factor with two levels (glycerol-treated, controls). The repeated measure was the series of measurements made on each mouse. The series had seven (or five) levels and was treated as a random effect. A significance level of 0.05 was used for all statistical calculations.

Recovery of a bone factor for each transcutaneous measurement followed previously described procedures.[40] An iterative background removal with a 5th-order polynomial was used to subtract the background fluorescence.[41, 42] The resulting spectra were normalized, the covariance matrix was calculated, and band target entropy minimization (BTEM)[40, 43, 44] was used to recover the spectral factors. A 3 cm^{-1} interval around the phosphate band (ca. 959 cm^{-1}) was chosen for band targeting. Between 3 and 23 eigenvectors from the data set were included for the calculation of Raman spectral factors. Eigenvectors containing predominantly random noise were used to improve the signal-to-noise ratio of the recovered bone spectra. An eigenvector weight distribution test for selecting the appropriate number of eigenvectors was used, as described elsewhere[40]. A stopping point was reached when additional eigenvectors added only noise.

Once the bone spectral factors were calculated, the cross-correlation coefficient between the bone factor and the exposed bone measurement was calculated using the ‘xcorr’ function of the Matlab signal processing toolbox. To exclude the intense P-O stretch, while including enough of the spectrum for computation, the interval used was 988–1500cm^{-1}. The mean cross-correlation coefficient was computed for the average of the spectra from each of the six tibiae. For each tibia, a paired t-test, as described above, was used to examine the difference in the cross-correlation coefficients between transcutaneous spectra measured with and without optical clearing. The effect of optical clearing on the correlation between transcutaneous and exposed bone measurements was tested for all six tibiae using a repeated measures ANOVA. Optical clearing was treated as a fixed factor with two levels (glycerol-treated, controls), and the repeated measure was the series of measurements on each mouse, which had seven (or five) levels and was treated as a random effect.

3 Results and Discussion

3.1 Noise Level Determined by Power Spectra

Transcutaneous Raman spectra taken through approximately 1mm of tissue on a mouse tibia are shown in Figure 2a. CCD white light correction, dark current subtraction, and correction of spectrograph-induced curvature was applied, but no further processing was done. The measurements made after glycerol application have visibly less intense and more reproducible background fluorescence than those from the control spectra, which were acquired prior to optical clearing. The power spectra for these Raman spectra are shown in Figure 2b. In the high transform frequency region (> 0.02 cycles/nm), where mostly noise is represented, the measurements made after optical clearing have both lower noise power and reduced measurement-to-measurement variability.

We attribute the spectroscopic effects of optical clearing to reduced specimen fluorescence in the acquired spectra. With 785 nm excitation the most important source of fluorescence is

melanin, which is located in the melanocytes. In mice, as in humans and other mammals the melanocytes lie just below the stratum corneum.[45] Decreasing the scattering at and just below the skin surface decreases the amount of fluorescence that is generated and the amount reaching the collection fibers, thereby decreasing its contribution to the total collected signal. Some photobleaching may also be occurring during the first few minutes of laser illumination. The background decreases rapidly between the first and second spectrum acquisition but slowly thereafter (Figure 2a).

Bar graphs of noise levels and measurement variability for each tibia are shown in Figure 3a. The measurements taken after optical clearing had a significantly lower noise level ($p<0.05$) in 4 out of the 6 tibiae. In addition, the variability in a set of spectra, indicated by the error bars, was lower for spectra acquired after the application of glycerol, although the differences were not statistically significant in tibiae 2 and 6. The mean noise levels for the six tibiae are presented in Figure 3b. The spectra acquired after optical clearing have significantly less noise ($p=0.0037$).

Recovery of the bone spectrum depends on separation of the bone component from that of the overlying tissue, which includes skin, tendon, blood vessels and even some adipose tissue. Optical clearing can actually degrade the recovered bone spectrum if the fiber optic probe is not aligned so as to maximize the contribution from bone and minimize the contribution from overlying tissue. This effect is illustrated in Figure 4. The illumination line must be positioned directly over the bone, and the collection fibers must be centered on this line, as shown in Figure 4a. The field of view of the collection fibers is then as illustrated in Figure 4b.

However, if the collection fibers are not positioned directly over the bone and centered on the illumination line, spectra from soft tissue are over-sampled. We demonstrated these effects by misaligning the probe. The field of view of the collection fibers was shifted toward the medial side of the tibia while the illumination line centered over the bone. The improper collection fiber alignment is shown in Figure 4c. The rms noise for the control and optical clearing cases are shown in Figure 4d. Significantly more noise was observed in the measurement made after glycerol application ($p<0.00001$). This seemingly contradictory result is caused by the reduction of light scattering by the skin, allowing oversampling of Raman scatter from the soft tissue directly below. As expected, the overall intensity of the bone component of the recovered spectrum is decreased. The effect is seen most clearly in the phosphate ν_1 band at 959 cm^{-1} (Figure 4e). The absolute intensity of the phosphate ν_1 band recovered with the misaligned probe is not as great as that obtained when the probe is properly aligned. Because the signal-to-noise ratio is reduced and the contribution from skin and tendon collagen is increased by probe misalignment, the accuracy of the recovered bone factor is also lowered.

3.2 Cross-correlation Coefficients

The cross-correlation coefficients between bone factors recovered from transcutaneous and exposed bone spectra further illustrate the effects of optical clearing. Because in the mouse tibia the bone lies only about 1 mm below the skin, a strong phosphate ν_1 band is actually visible in the spectrum, after removal of fluorescence background (Figure 5). The Raman spectrum of type I collagen in skin and tendon is similar to that of type I collagen in bone. As a consequence the collagen bands are much more intense than the similar bands in exposed bone, as comparison to the exposed bone spectrum shows. Collagen bands near the 1070 cm^{-1} region effectively mask the carbonate ν_1 band at 1070 cm^{-1}. By reducing the skin collagen contribution, optical clearing with glycerol improves the accuracy of the recovered bone factor, as shown in Figure 5b. The difference is clearest in the less intense bands.

To quantify the difference between the recovered bone factors and the exposed bone measurements, cross-correlation coefficients were calculated in the low signal-to-noise portion

of the recovered spectra, i.e., excluding the phosphate ν_1 band (Figure 6). The spectra acquired after optical clearing had a significantly higher correlation with the exposed bone spectra ($p<0.07$) in 4 of the 6 tibiae. The mean cross-correlation coefficients are shown in Figure 6b. The measurements made after optical clearing have a significantly higher correlation with the exposed bone spectra ($p=0.025$) than those of controls, without optical clearing.

4 Conclusions

Optical clearing improves the signal-to-noise ratio of transcutaneously measured bone Raman spectra. Our initial experiments employed only one clearing agent, glycerol, and a simple protocol. Glycerol was chosen, because it is known to be effective and safe for use on humans. Other clearing agents and application protocols may prove even more effective. For example, dermabrasion to remove a portion of the stratum corneum is known to improve penetration of clearing agents. Compression or stretching of the skin has also been shown to improve light transmission.[10] The use of one or more of these techniques should allow transcutaneous measurement of bone Raman spectra with an even better signal-to-noise ratio.

Further development of the line-focused probe could also improve the performance of the system. The available Powell lens assembly was not coated for 785 nm, nor was its internal collimator adjustable to correct for beam divergence. As a result, throughput was reduced. The delivered power was 35 mW from a 400 mW laser. Unlike the ring/disk system, the present configuration does not allow for adjustment of the distance between the entry and collection points. Moreover, the collection fibers are arranged in a disk, resulting in undersampling of the offset points at the periphery of the field of view. These problems can be mitigated with a rectangular collection fiber array and line-forming optics that are designed to work properly with the 785 nm output from a multimode optical fiber. Development of this system is underway, and its performance will be reported at a later date.

Acknowledgments

The authors acknowledge support through NIH grant R01 AR052010 and by the University of Michigan Musculoskeletal Core Research Center, NIH grant P30 AR46024 and University of Michigan Claude D. Pepper Older Americans Independence Center AG014824. J.H.C acknowledges support through an NIH Kirschstein-NRSA T90 DK070071-03, and K.A.D. acknowledges support through NIH training grant T32 GM008353.

References

1. Kozloff KM, Carden A, Bergwitz C, Forlino A, Uveges TE, Morris MD, Marini JC, Goldstein SA. Brittle IV Mouse Model for Osteogenesis Imperfecta IV Demonstrates Postpubertal Adaptations to Improve Whole Bone Strength. J. Bone Miner. Res 2004;19(4):614–622. [PubMed: 15005849]
2. Tarnowski CP, I MA Jr, Morris MD. Mineralization of Developing Mouse Calvaria as Revealed by Raman Microspectroscopy. J. Bone Miner. Res 2002;17(6):1118–1126. [PubMed: 12054168]
3. Tarnowski CP, I MA Jr, Wang W, Taboas JM, Goldstein SA, Morris MD. Earliest Mineral and Matrix Changes in Force-Induced Musculoskeletal Disease as Revealed by Raman Microspectroscopic Imaging. J. Bone Miner. Res 2004;19(1):64–71. [PubMed: 14753738]
4. Kohn DH, Sahar ND, Hong SI, Golcuk K, Morris MD. Local Mineral and Matrix Changes Associated with Bone Adaptation and Microdamage. Mater. Res. Soc. Symp. Proc 2006;898E(L0903):1–11.
5. Carden A, Rajachar RM, Morris MD, Kohn DH. Ultrastructural Changes Accompanying the Mechanical Deformation of Bone Tissue: A Raman Imaging Study. Calcif. Tissue Int 2003;72:166–175. [PubMed: 12469250]
6. Chen T-C, Kozloff K, Goldstein S, Morris M. Bone Tissue Ultrastructural Deffects in a mouse model for Osteogenesis Imperfecta: a Raman Spectroscopy Study. Proc. SPIE 2004;5321:85.
7. Faibish D, Ott SM, Boskey AL. Mineral Changes in Osteoporosis a Review. Clin. Orthop. Relat. Res 2006;443:28–38. [PubMed: 16462423]

8. McCreadie BR, Morris MD, Chen T-C, Rao DS, Finney WF, Widjaja E, Goldstein SA. Bone Extracellular Matrix Compositional Differences in Women with and without Osteoporotic Fracture. Bone 2006;39:1190–1195. [PubMed: 16901772]
9. Dehring KA, Crane NJ, Smukler AR, McHugh JB, Roessler BJ, Morris MD. Identifying Chemical Changes in Subchondral Bone Taken from Murine Knee Joints Using Raman Spectroscopy. Appl. Spectrosc 2006;60(10):1134–1141. [PubMed: 17059665]
10. Tuchin VV. Optical Clearing of Tissue and Blood. 2006
11. Eikje NS, Ozaki Y, Aizawa K, Arase S. Fiber optic near-infrared Raman spectroscopy for clinical noninvasive determination of water content in diseased skin and assessment of cutaneous edema. J. Biomed. Opt 2005;10(1):14013. [PubMed: 15847594]
12. Caspers PJ, Lucassen GW, Puppels* GJ. Combined In Vivo Confocal Raman Spectroscopy and Confocal Microscopy of Human Skin. Biophys. J 2003 July;85:572–580. [PubMed: 12829511]
13. Hammond BR, Wooten BR. Resonance Raman spectroscopic measurement of carotenoids in the skin and retina. J. Biomed. Opt 2005;10(5):054002. [PubMed: 16292962]
14. Caspers PJ, Williams AC, Carter EA, Edwards HGM, Barry BW, Bruining HA, Puppels GJ. Monitoring the Penetration Enhancer Dimethyl Sulfoxide in Human Stratum Corneum in Vivo by Confocal Raman Spectroscopy. Pharm. Res 2002;19(10):1577–1580. [PubMed: 12425479]
15. Song Y, Xiao C, Mendelsohn R, Zheng T, Strekowski L, Michniak B. Investigation of iminosulfuranes as novel transdermal penetration enhancers: enhancement activity and cytotoxicity. Pharm. Res 2005;22(11):1918–1925. [PubMed: 16132348]
16. Motz JT, Fitzmaurice M, Miller A, Gandhi SJ, Haka AS, Galindo LH, Dasari RR, Kramer JR, Feld MS. In vivo Raman spectral pathology of human atherosclerosis and vulnerable plaque. J. Biomed. Opt 2006;11(2):021003. [PubMed: 16674178]
17. Motz JT, Gandhi SJ, Scepanovic OR, Haka AS, Kramer JR, Dasari RR, Feld MS. Real-time Raman system for in vivo disease diagnosis. J. Biomed. Opt 2005;10(3):031113. [PubMed: 16229638]
18. Scepanovic OR, Fitzmaurice M, Gardecki JA, Angheloiu GO, Awasthi S, Motz JT, Kramer JR, Dasari RR, Feld MS. Detection of morphological markers of vulnerable atherosclerotic plaque using multimodal spectroscopy. J. Biomed. Opt 2006;11(2):021007. [PubMed: 16674182]
19. Enejder AMK, Koo T-W, Oh J, Hunter M, Sasic S, Feld MS. Blood analysis by Raman spectroscopy. Opt. Let 2003;27(22):2004–2006. [PubMed: 18033426]
20. Enejder AMK, Scecina TG, Oh J, Hunter M, Shih W-C, Sasic S, Horowitz GL, Feld MS. Raman spectroscopy for noninvasive glucose measurements. J. Biomed. Opt 2005;10(3):031114. [PubMed: 16229639]
21. Pilotto S, Pacheco MTT, S L Jr, Villaverde AB, Zaˆngaro RA. Analysis of Near-infrared Raman Spectroscopy as a New Technique for a Transcutaneous Non-invasive Diagnosis of Blood Components. Lasers Med. Sci 2001;16(1):2–9. [PubMed: 11486334]
22. Yeh AT, Hirshburg J. Molecular interactions of exogenous chemical agents with collagen—implications for tissue optical clearing. J. Biomed. Opt 2006;11(1):014003. [PubMed: 16526880]
23. Cicchi R, Massi D, Stambouli D, Sampson DD, Pavone FS. Contrast enhancement in combined two-photon second harmonic imaging of skin by using hyperosmotic agents. Proc. SPIE 2006;6089 60890X.
24. Xu X, Wang RK. The role of water desorption on optical clearing of biotissue: Studied with near infrared reflectance spectroscopy. Med. Phys 2003;30(6):1246–1253. [PubMed: 12852550]
25. He Y, Wang RK. Dynamic optical clearing effect of tissue impregnated with hyperosmotic agents and studied with optical coherence tomography. J. Biomed. Opt 2004;9(1):200–206. [PubMed: 14715074]
26. Yeh AT, Choi B, Nelson JS, Tromberg BJ. Reversible Dissociation of Collagen in Tissues. J.Invest. Derm 2003;121(6):1332–1335. [PubMed: 14675178]
27. Matousek P, CLark IP, Draper ERC, Morris MD, Goodship AE, Everall N, Towrie M, Finney WF, Parker AW. Subsurface Probing in Diffusely Scattering Media Using Spatially Offset Raman Spectroscopy. Appl. Spectrosc 2005;59(4):393–400. [PubMed: 15901323]
28. Matousek P, Morris MD, Everall N, Clark IP, Towrie M, Draper E, Goodship A, Parker AW. Numerical Simulations of Subsurface Probing in Diffusely Scattering Media Using Spatially Offset Raman Spectroscopy. Appl. Spectrosc 2005;59(12):1485–1492. [PubMed: 16390587]

29. Schulmerich MV, Finney WF, Popescu V, Morris MD, Vanasse TM, Goldstein SA. Transcutaneous Raman spectroscopy of bone tissue using a nonconfocal fiber optic array probe. Proc. SPIE 2006;6093:O1–O7.
30. Schulmerich MV, Finney WF, Fredricks RA, Morris MD. Subsurface Raman Spectroscopy and Mapping Using a Globally Illuminated Non-Confocal Fiber-Optic Array Probe in the Presence of Raman Photon Migration. Appl. Spectrosc 2006;60(2):109–114. [PubMed: 16542561]
31. Schulmerich MV, Dooley KA, Morris MD, Vanasse TM, Goldstein SA. Transcutaneous fiber optic Raman spectroscopy of bone using annular illumination and a circular array of collection fibers. J. Biomed. Opt 2006;11(6):060502. [PubMed: 17212521]
32. Schulmerich MV, Morris MD, Vanasse TM, Goldstein SA. Transcutaneous Raman spectroscopy of bone: global sampling and ring/disk fiber optic probes. Proc. SPIE 2007;6430(643009):1–8.
33. Matousek P. Inverse Spatially Offset Raman Spectroscopy for Deep Noninvasive Probing of Turbid Media. Appl. Spectrosc 2006;60(11):1341–1347. [PubMed: 17132454]
34. Schulmerich MV, Dooley KA, Vanasse TM, Goldstein SA, Morris MD. Subsurface and Transcutaneous Raman Spectroscopy andMapping Using Concentric Illumination Rings and Collection with a Circular Fiber-Optic Array. Appl. Spectrosc 2007;61(7) in press.
35. Richards-Kortum R, Sevick-Muraca E. Quantitative Optical Spectroscopy for Tissue Disagnosis. An. Rev. Phys. Chem 1996;47:555–606.
36. Tuchin V. Tissue Optics Light Scattering Methods and Instruments for Medical Diagnosis. 2000
37. Vo-Dinh, T. Biomedical Photonics Handbook. 2003.
38. Carden A, Morris MD. Application of vibrational spectroscopy to the study of mineralized tissues (review). J. Biomed. Opt 2000;5(3):259–268. [PubMed: 10958610]
39. Devore, JL. Probability and statistics for engineering and the sciences. Toronto: Thomson Brooks/ Cole; 2004.
40. Widjaja E, Crane N, Chen T-C, Morris MD, Ignelzi MA, McCreadie BR. Band-Target Entropy Minimization (BTEM) Applied to Hyperspectral Raman Image Data. Appl. Spectrosc 2003;57(11): 1353–1362. [PubMed: 14658148]
41. Leger M, Ryder A. Comparison of Derivative Preprocessing and Automated Polynomial Baseline Correction Method for Classification and Quantification of Narcotics in Solid Mixtures. Appl. Spectrosc 2006;60(2):182–193. [PubMed: 16542570]
42. Lieber CA, Mahadevan-Jansen A. Automated Method for Subtraction of Fluorescence from Biological Raman Spectra. Appl. Spectrosc 2003;57(11):1363–1367. [PubMed: 14658149]
43. Chew W, Widjaja E, Garland M. Band-Target Entropy Minimization (BTEM): An Advanced Method for Recovering Unknown Pure Component Spectra. Application to the FTIR Spectra of Unstable Organometallic Mixtures. Organometallics 2002;21:1982–1990.
44. Widjaja E, Li C, Garland M. Semi-Batch Homogeneous Catalytic In-Situ Spectroscopic Data. FTIR Spectral Reconstructions Using Band-Target Entropy Minimization (BTEM) without Spectral Preconditioning. Organometallics 2002;21:1991–1997.
45. Briggaman RA, Wheeler CE Jr. The Epidermal-Dermal Junction. J. Invest. Derm 1975;65(1):71–84. [PubMed: 1097542]

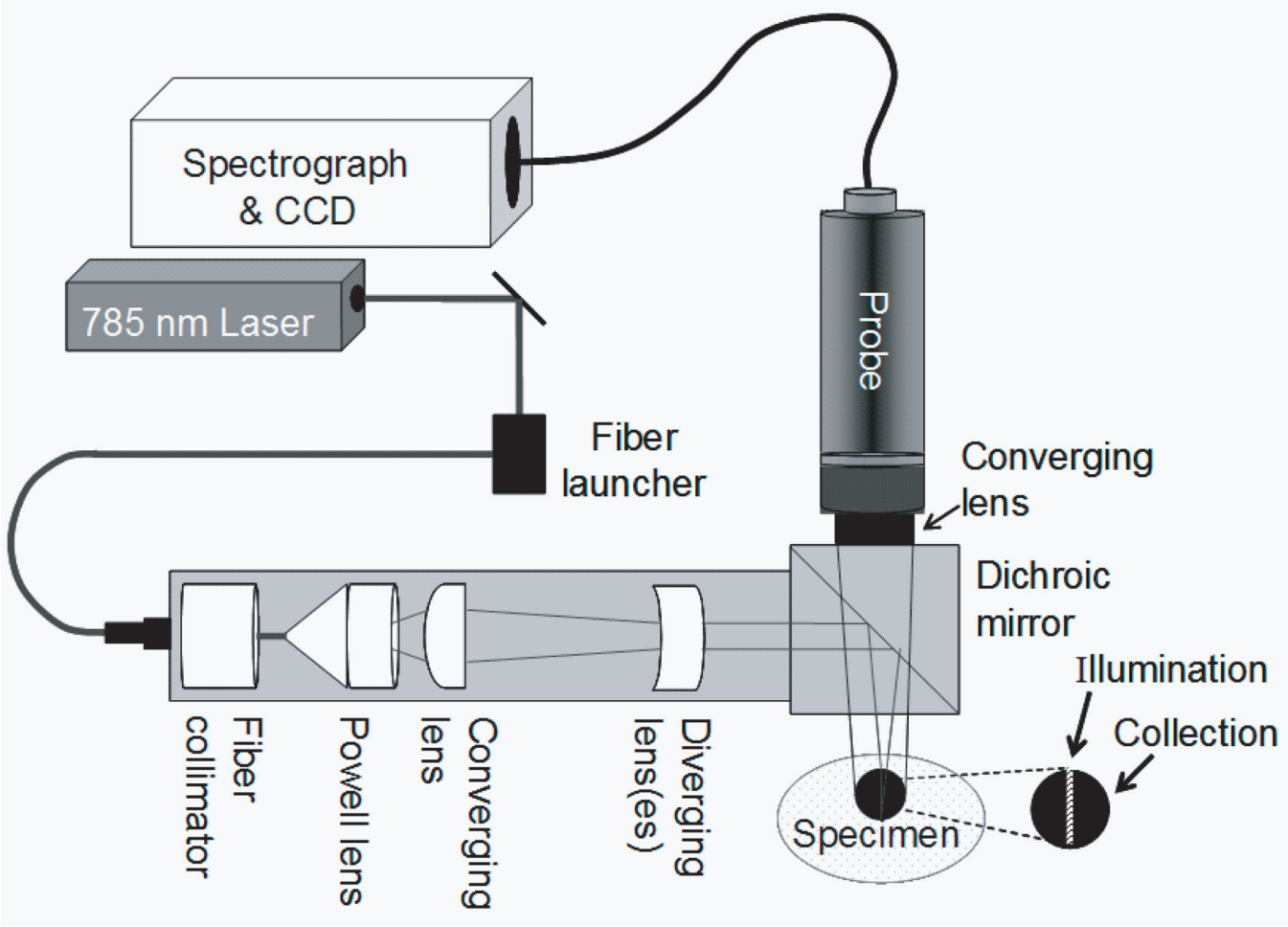

Fig. 1.
Schematic of experimental apparatus

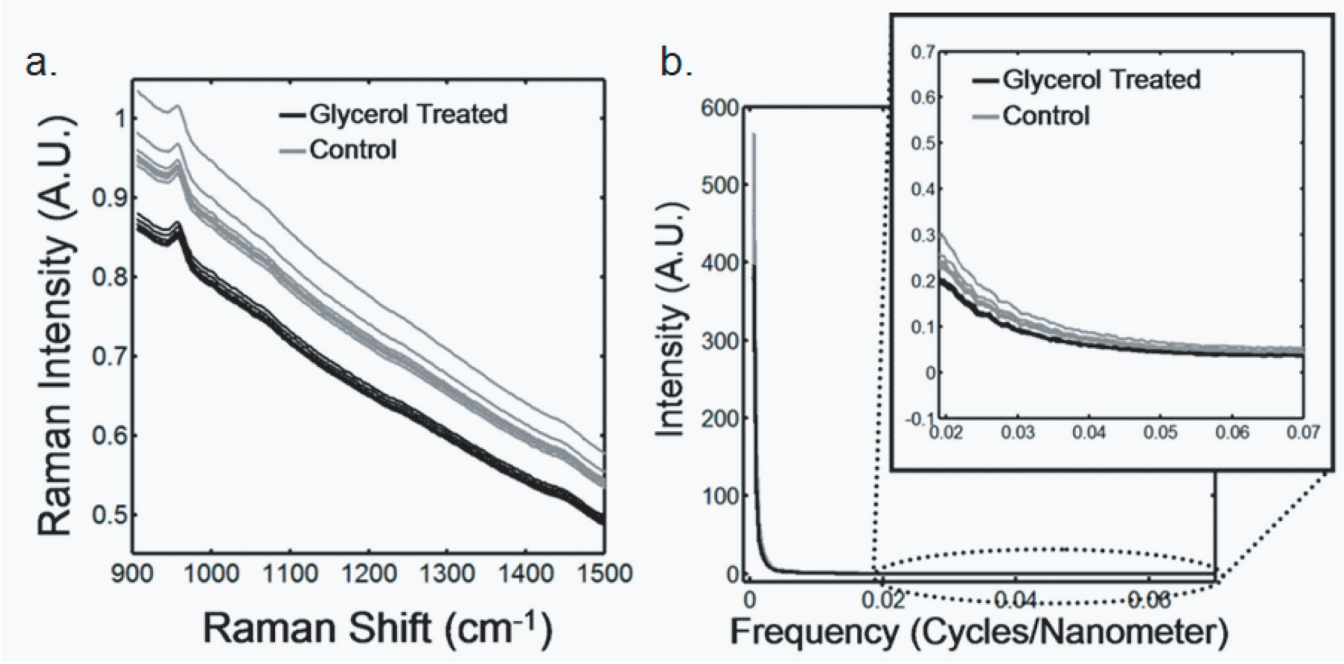

Fig. 2.

Raman spectra of a murine tibia (distal diaphysis). The bone tissue is approximately 1 mm below the skin. The gray traces are raw spectra obtained without optical clearing, and the black traces are spectra obtained after glycerol application (a) Transcutaneous Raman spectra (b) Power spectra

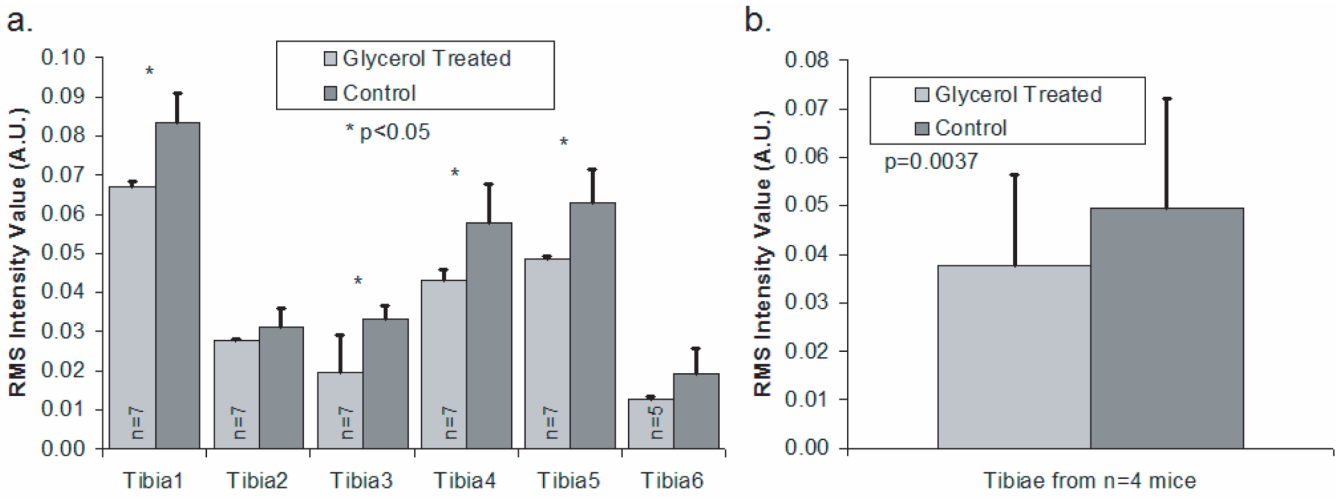

Fig. 3.

rms intensity for power spectra in high transform frequency region (mean + standard deviation) (a) Results for measurements made on six different tibiae (b) Results across tibiae from all mice

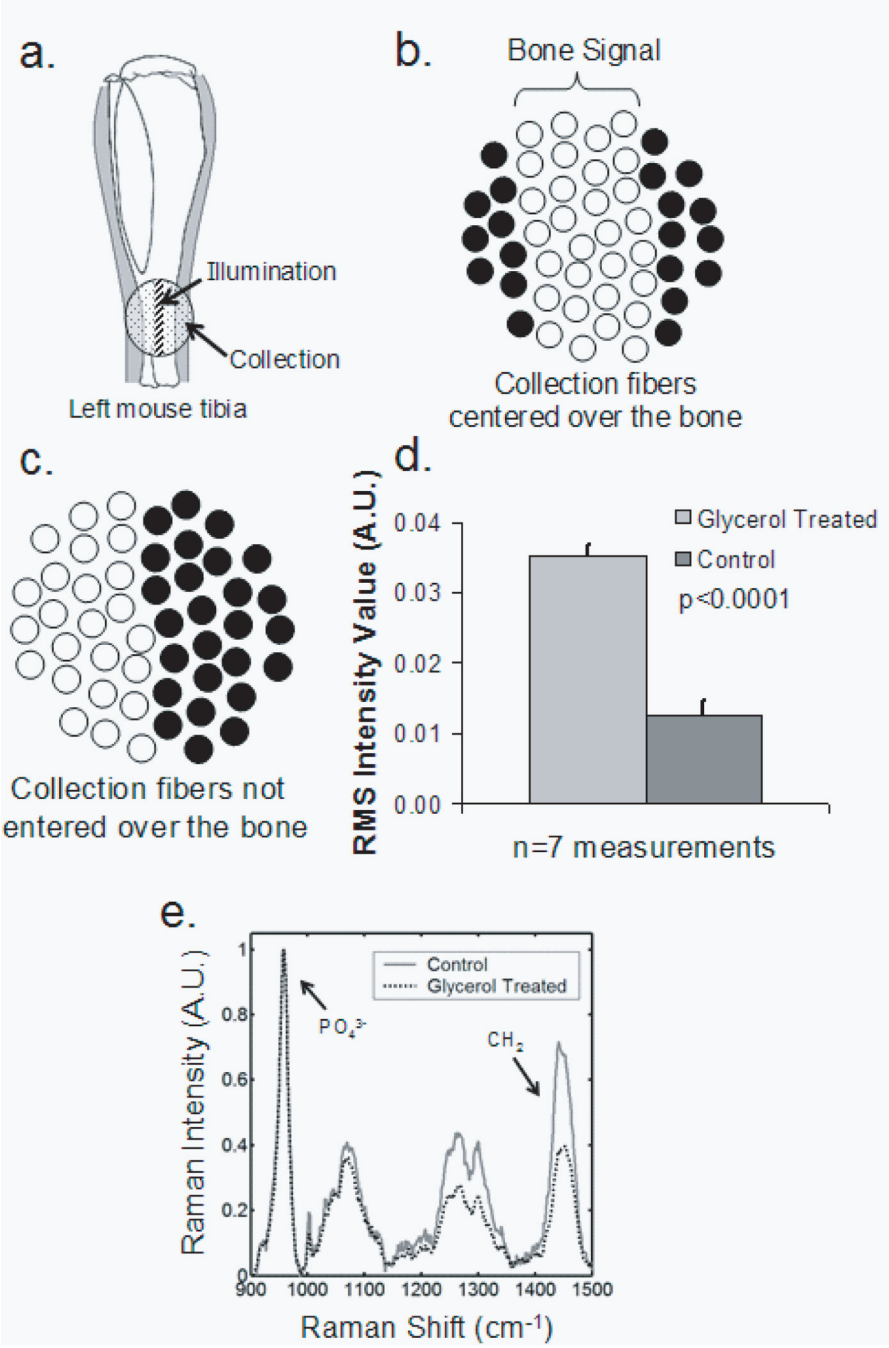

Fig. 4.

Effect of not centering the illumination line in the center of the collection fibers (a) Correct alignment of illumination line and collection disk with respect to the bone (b) Field of view of the collection fibers for proper alignment (c) Field of view of the collection fibers for improper alignment (d) Resulting noise levels in measurements made with improper alignment (compare to Fig. 3) (e) Mean transcutaneous spectra, after baselining and normalizing, for a measurement before and after glycerol application

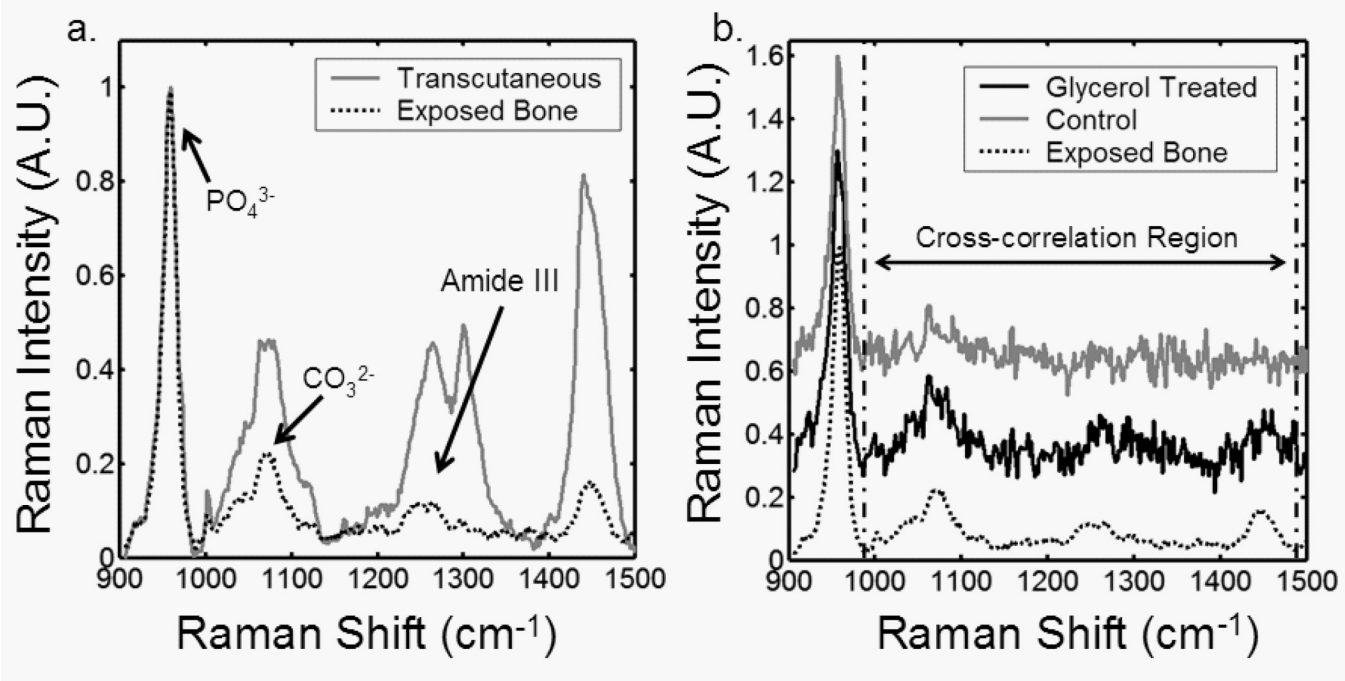

Fig. 5.

(a) Typical mean transcutaneous spectrum (gray) and typical mean exposed bone spectrum (black) (b) Recovered bone factor without an optical clearing agent (gray), recovered bone factor after glycerol application (black), and exposed bone measurement (dotted)

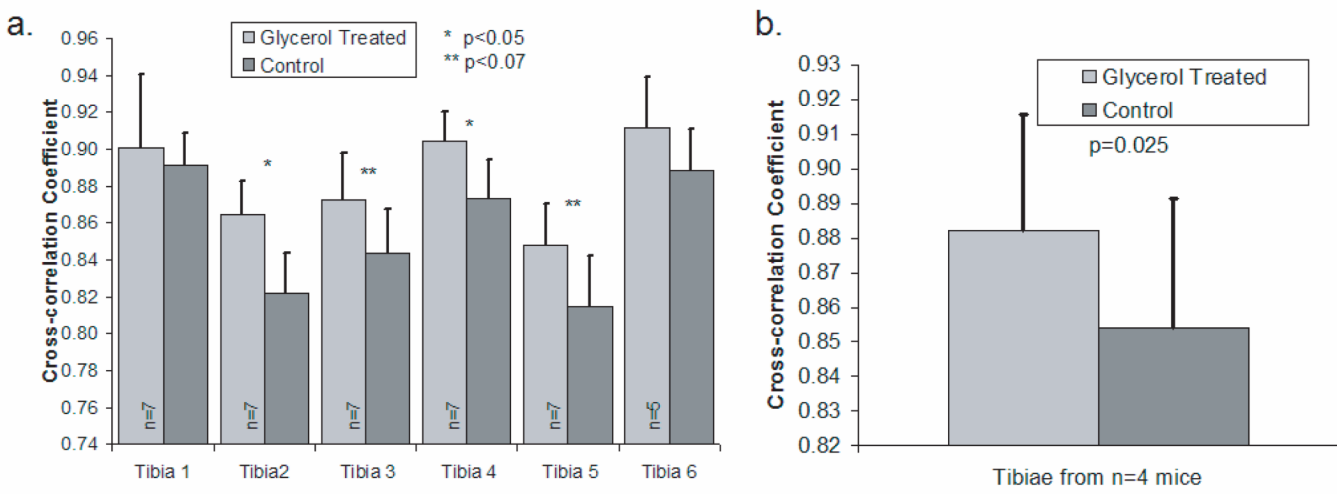

Fig. 6.

Cross-correlation coefficient between the exposed bone measurement and the recovered bone factor (mean + standard deviation) (a) Results for measurements made on six different tibiae (b) Results across tibiae from all mice